



## OPEN ACCESS

## EDITED BY

Silvia Capuani,  
National Research Council (CNR), Italy

## REVIEWED BY

Bram F. Coolen,  
University of Amsterdam, Netherlands  
Christian Herbert Ziener,  
German Cancer Research Center  
(DKFZ), Germany

## \*CORRESPONDENCE

Ali Nahardani,  
Nahardani.ali@gmail.com  
Verena Hoerr,  
vhoerr@uni-bonn.de

## SPECIALTY SECTION

This article was submitted to Medical  
Physics and Imaging,  
a section of the journal  
Frontiers in Physics

RECEIVED 07 June 2022

ACCEPTED 05 September 2022

PUBLISHED 27 September 2022

## CITATION

Nahardani A, Krämer M, Ebrahimi M,  
Herrmann K-H, Leistikow S, Linsen L,  
Moradi S, Reichenbach JR and Hoerr V  
(2022), Time-resolved velocity mapping  
at high magnetic fields: A preclinical  
comparison between stack-of-stars and  
cartesian 4D-Flow.

*Front. Phys.* 10:963807.

doi: 10.3389/fphy.2022.963807

## COPYRIGHT

© 2022 Nahardani, Krämer, Ebrahimi,  
Herrmann, Leistikow, Linsen, Moradi,  
Reichenbach and Hoerr. This is an  
open-access article distributed under  
the terms of the [Creative Commons  
Attribution License \(CC BY\)](https://creativecommons.org/licenses/by/4.0/). The use,  
distribution or reproduction in other  
forums is permitted, provided the  
original author(s) and the copyright  
owner(s) are credited and that the  
original publication in this journal is  
cited, in accordance with accepted  
academic practice. No use, distribution  
or reproduction is permitted which does  
not comply with these terms.

# Time-resolved velocity mapping at high magnetic fields: A preclinical comparison between stack-of-stars and cartesian 4D-Flow

Ali Nahardani<sup>1,2\*</sup>, Martin Krämer<sup>1,3</sup>, Mahyasadat Ebrahimi<sup>4,5</sup>,  
Karl-Heinz Herrmann<sup>1</sup>, Simon Leistikow<sup>6</sup>, Lars Linsen<sup>6</sup>,  
Sara Moradi<sup>2</sup>, Jürgen R. Reichenbach<sup>1</sup> and Verena Hoerr<sup>1,2,7\*</sup>

<sup>1</sup>Medical Physics Group, Institute of Diagnostic and Interventional Radiology, Jena University Hospital, Friedrich Schiller University Jena, Jena, Germany, <sup>2</sup>Heart Center Bonn, Department of Internal Medicine II, University Hospital Bonn, Bonn, Germany, <sup>3</sup>Institute of Diagnostic and Interventional Radiology, Jena University Hospital, Friedrich Schiller University Jena, Jena, Germany, <sup>4</sup>Leibniz-Institute of Photonic Technology, Jena, Germany, <sup>5</sup>Institute of Physical Chemistry and Abbe Center of Photonics, Friedrich Schiller University Jena, Jena, Germany, <sup>6</sup>Department of Mathematics and Computer Science, Institute of Computer Science, Westfälische Wilhelms-Universität Münster, Münster, Germany, <sup>7</sup>Translational Research Imaging Center (TRIC), Clinic of Radiology, University of Münster, Münster, Germany

**Purpose:** Prospectively-gated Cartesian 4D-flow (referred to as Cartesian-4D-flow) imaging suffers from long TE and intensified flow-related intravoxel-dephasing especially in preclinical ultra-high field MRI. The ultra-short-echo (UTE) 4D-flow technique can resolve the signal loss in higher-order blood flows; however, the long scan time of the high resolution UTE-4D-flow is considered as a disadvantage for preclinical imaging. To compensate for prolonged acquisitions, an accelerated  $k_0$ -navigated golden-angle center-out stack-of-stars 4D-flow sequence (referred to as SoS-4D-flow) was implemented at 9.4T and the results were compared to conventional Cartesian-4D-flow mapping *in-vitro* and *in-vivo*.

**Methods:** The study was conducted in three steps (A) *In-vitro* evaluation in a static phantom: to quantify the background velocity bias. (B) *In-vitro* evaluation in a flowing water phantom: to investigate the effects of polar undersampling (US) on the measured velocities and to compare the spatial velocity profiles between both sequences. (C) *In-vivo* evaluations: 24 C57BL/6 mice were measured by SoS-4D-flow ( $n = 14$ ) and Cartesian-4D-flow ( $n = 10$ ). The peak systolic velocity in the ascending aorta and the background velocity in the anterior chest wall were analyzed for both techniques and were compared to each other.

**Results:** According to the *in-vitro* analysis, the background velocity bias was significantly lower in SoS-4D-flow than in Cartesian-4D-flow ( $p < 0.05$ ). Polar US in SoS-4D-flow influenced neither the measured velocity values nor the spatial velocity profiles in comparison to Cartesian-4D-flow. The *in-vivo* analysis showed significantly higher diastolic velocities in Cartesian-4D-flow than in SoS-4D-flow ( $p < 0.05$ ). A systemic background bias was observed in the

Cartesian velocity maps which influenced their streamline directions and magnitudes.

**Conclusion:** The results of our study showed that at 9.4T SoS-4D-flow provided higher accuracy in slow flow imaging than Cartesian-4D-flow, while the same measurement time could be achieved.

KEYWORDS

MRI, 4D-flow, phase-contrast, stack-of-stars, UTE

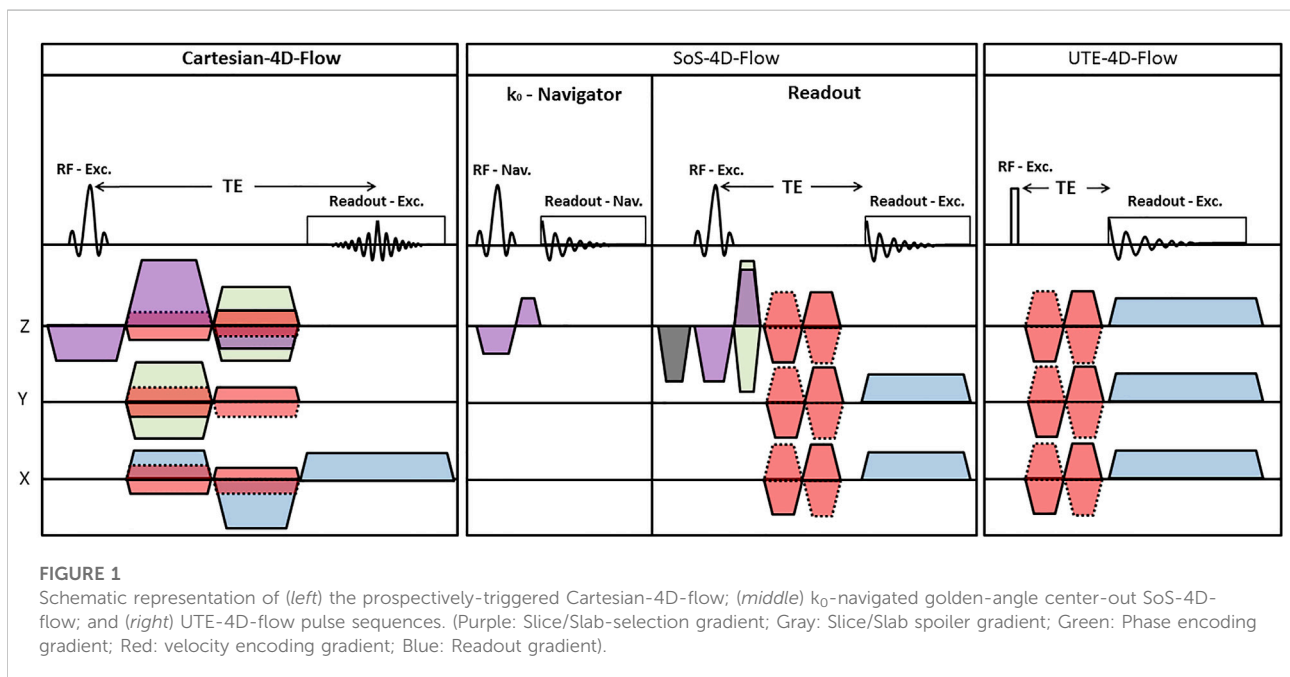
# 1 Introduction

4D phase contrast magnetic resonance imaging, commonly known as 4D-flow, is a technique in cardiovascular MRI for quantifying blood velocity in the 3D space along time [1]. For this purpose, multiple sets of bipolar velocity encoding gradients are applied 3D to sensitize the MRI signal to fast moving spins [2]. Since the quantification of the velocity requires a baseline measurement to subtract the phase of the signal of the dynamic spins, a variety of velocity encoding methods have been emerged which differ in their number of gradients and in accuracy. However, the imbalanced and balanced 4-point methods have become popular since they require the least number of gradients while exhibiting low bias [3–5].

The type of velocity encoding scheme is not the only factor influencing the accuracy of the measured velocity maps. It has been shown that the k-space trajectory has also an impact on accuracy, especially at ultra-high-fields (UHF) [3, 6, 7].

Basically, 4D-flow imaging using Cartesian trajectory has been extensively investigated not only at low fields [8], but also at UHFs [9, 10]. It has been widely used in preclinical MRI (i.e., at

UHFs) and benefits from a simple reconstruction pipeline which is compatible with the existing acceleration techniques [8, 11]. However, acceleration by means of the partial coverage of the k-space can influence the accuracy of the velocity maps that may not be recoverable by advanced reconstruction algorithms (such as compressed sensing) [12]. Since the Cartesian trajectory requires multiple imaging gradients overlapping on each other, the gradient duty cycle of this technique is usually high. To tackle this problem, the gradients durations must be increased, influencing the minimum echo time (TE), which is typically >2–3 ms (Figure 1). Such a long TE can result in low signal-to-noise ratio (SNR), low velocity-to-noise ratio (VNR), and in an intensified signal loss in the disturbed flow at UHFs [6] which cannot even be resolved by shortening TE using asymmetric echo acquisition [3]. Moreover, the imaging encoding gradients in the 3D-Cartesian trajectory (i.e., the two phase encoding gradients, bipolar readout gradient, etc.) are experienced as extra velocity sensitizing gradients and result in a higher actual velocity encoding value (VENC) than the nominal value [13].



To increase the accuracy of velocity mapping at UHF, the ultra-short-echo (UTE) 4D-flow sequence has been introduced [3]. Since a very shortly durated rectangular radiofrequency (RF) pulse is applied in UTE-4D-flow and it requires no slice and phase encoding gradients, the corresponding TEs are sufficiently short ( $\approx 500 \mu\text{s}$ , Figure 1) to preserve the signal in the regions with higher-order blood flows [3]. Additionally, the center of the  $k$ -space is densely sampled in this technique; leading to a high SNR and VNR [3, 14–17]. UTE-4D-flow is also compatible with advanced acceleration techniques [7] but at the cost of higher complexity in reconstruction compared to the Cartesian data. Although the temporal resolution of UTE-4D-flow is superior to any Cartesian techniques (due to its typical shorter repetition time—TR), its total scan time is 9.8 times (i.e.,  $\pi^2$ ) longer to satisfy the Nyquist–Shannon sampling theorem for similar scan parameters, which is based on the fact that the coverage of radial spokes should create equidistant solid angles by  $\pi$  projections along the  $k_z$  direction and  $2\pi$  projections in the  $k_{xy}$  plane.

Moreover, the choice of the gating strategy can influence the total scan time and the quality of velocity maps; especially in small animals due to their rapid heart and respiratory rates. For preclinical imaging at UHF, the gating efficiency of the prospective triggering method has been reported to be about 50% because of the poor quality of electrocardiograms (ECG), the induction of noise by switching gradients, and long respiratory delays [3, 18]; nonetheless, it was improved to around 60% in self-gating [3].

When aiming for 4D-flow imaging with reasonable spatial resolution, using the UTE-4D-flow technique is not justifiable due to its long scan time regardless of its very good image quality. To reduce the total scan time and still benefit from the advantages of UTE (i.e., short TE, high SNR, and high VNR), we implemented an efficient  $k_0$ -navigated golden-angle center-out stack-of-stars 4D phase-contrast imaging sequence (referred to as SoS-4D-flow in the context of this manuscript) as a hybrid combination of the half-spoke radial and Cartesian sampling techniques and investigated the results *in-vitro* and *in-vivo* in comparison to those obtained by the conventional prospectively-triggered Cartesian-4D-flow method (called Cartesian-4D-flow in the following).

## 2 Methods

### 2.1 Imaging experiments

#### 2.1.1 *In-vitro*

Two types of phantoms were used for the evaluations (A) Static water phantom, i.e., a simple 50 ml conical tube filled with agar and a small Lego brick inside; (B) Flowing water phantom, i.e. a large cylinder with the inner diameter of 26.1 mm containing water and enclosing four smaller tubes with the inner diameter of 3 mm, which are connected to a water pump with adjustable flow rates of 0, 200,

400, 600, 800 ml/s to produce laminar flows with different speeds. Imaging was carried out on a 9.4T BioSpec USR 94/20 MRI system with ParaVision 6.0.1 (Bruker BioSpin MRI GmbH, Ettlingen, Germany) using a vendor-supplied 72-mm-diameter transmitter and receiver volume coil with the sequences and parameters listed in Table 1.

#### 2.1.2 *In-vivo*

24 male C57BL/6 mice were included in the study and divided into two experimental groups (A) 10 animals were scanned with the prospectively-triggered Cartesian-4D-flow sequence; (B) 14 animals were investigated with the  $k_0$ -navigated golden-angle SoS-4D-flow technique. It is important to note that SoS-4D-flow was performed by 25 repetitions for retrospective reconstruction and 2.5 undersampling factor (US). A summary of the sequences and parameters is provided in Table 1. All acquisitions were performed with the same hardware settings as in the *in-vitro* step, except for the coil; a dedicated cardiac 4-channel phased-array was used as receiver instead of the 72 mm Quadrature coil. The study was performed in accordance with the National Institute of Health Guidelines for the Care and Use of Laboratory Animals (eighth edition) and the European Community Council Directive for the Care and Use of Laboratory Animals of 22 September 2010 (2010/63/EU). The study protocol was approved by the competent State Office for Food Safety and Consumer Protection (TLLV, Bad Langensalza, Germany; local registration number: 22-2684-04-UKJ-19-002).

## 2.2 Pulse sequences

### 2.2.1 SoS-4D-flow

The  $k_0$ -navigated golden-angle center-out stack-of-stars 4D phase-contrast velocity mapping was implemented in five steps (A) A vendor-supplied 2D-UTE sequence with ramp-sampling was modified by integrating a 3D phase-encoding gradient along the slice/slab-selection direction to turn it into a 3D-SoS. To shorten TE, the phase encoding gradient was overlapped with the slice/slab-selection rephasing gradient. No phase rewinder gradient was added to reduce TR. (B) The readout spoiler gradient was removed from the sequence; instead, a short and strong slice/slab spoiler gradient was applied next to the slice/slab-selection gradient before the next excitation to compensate for any interference artifacts that could arise in its absence. (C) After the development of a stable version of 3D-SoS with a continuous rotation angle, the golden angle acquisition (with the rotation angle of  $\pi(3-\sqrt{5}) = 137.507$  between spokes) was integrated in the sequence, which guaranteed good  $k$ -space coverage even at high US factors. (D) To retrospectively sort the radial spokes with respect to the physiological motion, an external  $k_0$ -navigator module was implemented just before the main acquisition block of the sequence. In  $k_0$ -navigator, a slice-selective short-duration RF-pulse (0.1024 ms) was applied in an arbitrary (user-specified) orientation. The corresponding FID signal was collected in the absence of gradients, which was primarily

TABLE 1 Summary of the applied sequences and their corresponding parameters.

Sequence	TR/TE (ms)	FA (°)	BW (kHz)	US	NRep	Res ( $\mu\text{m}^3$ )	VENC (cm/s)	Receiver coil
<i>In-Vitro</i>								
Cartesian-4D-flow	6.0/1.8	4.0	100	1	1	$300 \times 300 \times 300$	20-800	72mm Quadrature
SoS-4D-flow	6.0/1.0	4.0	100	1-8	1	$300 \times 300 \times 300$	20-800	72mm Quadrature
<i>In-Vivo</i>								
Cartesian-4D-flow	6.0/1.8	4.0	100	1	1	$230 \times 230 \times 230$	85	4-channel Phase Array
SoS-4D-flow	6.0/1.0	4.0	100	2.5	25	$230 \times 230 \times 230$	85	4-channel Phase Array

(TR, repetition time; TE, echo time; FA, flip angle; BW, bandwidth; US, undersampling factor; NRep, number of repetitions; Res, resolution; VENC, velocity encoding value).

modulated by the cardiac and/or diaphragmatic motion. (E) The balanced 4-point velocity encoding scheme was integrated in the sequence just after the 3D phase-encoding gradient to sensitize the center-out radial spokes to higher-order motion. The minimum duration of the flow-encoding gradient was calibrated to 0.6 ms as gradient imperfections arose at shorter intervals. After all modifications, a minimum TE  $\approx$  1 ms could be achieved. A schematic representation of the sequence is illustrated in Figure 1.

## 2.2.2 Cartesian-4D-flow

A commercially available prospectively-triggered Cartesian-4D-flow sequence (FlowMap, ParaVision 6.0.1, Bruker BioSpin MRI GmbH, Ettlingen, Germany) was used as a reference. The sequence was composed of a balanced 3D gradient-echo and a balanced 4-point velocity encoding scheme. A respiratory bulb and a 3-lead ECG were used to capture the respiratory and cardiac motion and to prospectively synchronize the acquisition with physiological motion. The R-wave of the ECG during the expiratory period was set as the external trigger pulse. A schematic representation of the sequence is illustrated in Figure 1.

## 2.3 Image reconstruction

### 2.3.1 In-vitro data

#### 2.3.1.1 SoS-4D-flow

The imaging trajectory was measured by [19] before each acquisition. The corresponding k-space sampling densities were estimated using the trajectory information. The polar signals were gridded by an iterative sampling density compensation algorithm with optimized kernel using an in-house developed MATLAB framework. Finally, a 3D inverse fast Fourier operator (3D-iFFT) was applied on the gridded data to reconstruct the complex images. By the use of the complex images and the following equations, the individual velocity maps were calculated:

$$V_x = \angle \left( \frac{H_2 \circ H_3}{H_1 \circ H_4} \right) \quad (1)$$

$$V_y = \angle \left( \frac{H_2 \circ H_4}{H_1 \circ H_3} \right) \quad (2)$$

$$V_z = \angle \left( \frac{H_3 \circ H_4}{H_1 \circ H_2} \right) \quad (3)$$

Where  $H_i$  for  $i = 1-4$  stands for each HADAMARD velocity encoding imaging set.

#### 2.3.1.2 Cartesian-4D-flow

The *in-vitro* Cartesian-4D-flow data were reconstructed by the application of 3D-iFFT. The corresponding velocity maps were calculated using Eq 1-3.

### 2.3.2 In-vivo data

#### 2.3.2.1 $k_0$ -navigated SoS-4D-flow

For the *in-vivo* application of SoS-4D-flow, an external  $k_0$ -navigator was used. At first, different  $k_0$  signal components (i.e., magnitude, phase, imaginary, and real) were visually inspected to identify the optimal domain that best represented the cardiac and respiratory motion. Second, the navigator FID was amplified and summarized by taking the L2-norm of different channels. Third, FID was denoised by the Savitzky-Golay filter, and then the biorthogonal wavelet algorithm was applied to resolve the remaining signal redundancies. Fourth, the inspiration cycles were identified from FID, and the corresponding radial spokes were discarded. Fifth, by considering the peaks of FID as the onsets of the cardiac cycles, the radial signals were sorted according to the heart motion (Figure 2). Since many radial spokes were discarded in the process of retrospective reconstruction, a high degree of sparsity was achieved in the finally-sorted raw-data. Nonetheless, this problem could be resolved by averaging the sparse raw-data over all the acquired 25 repetitions (see the methods section).

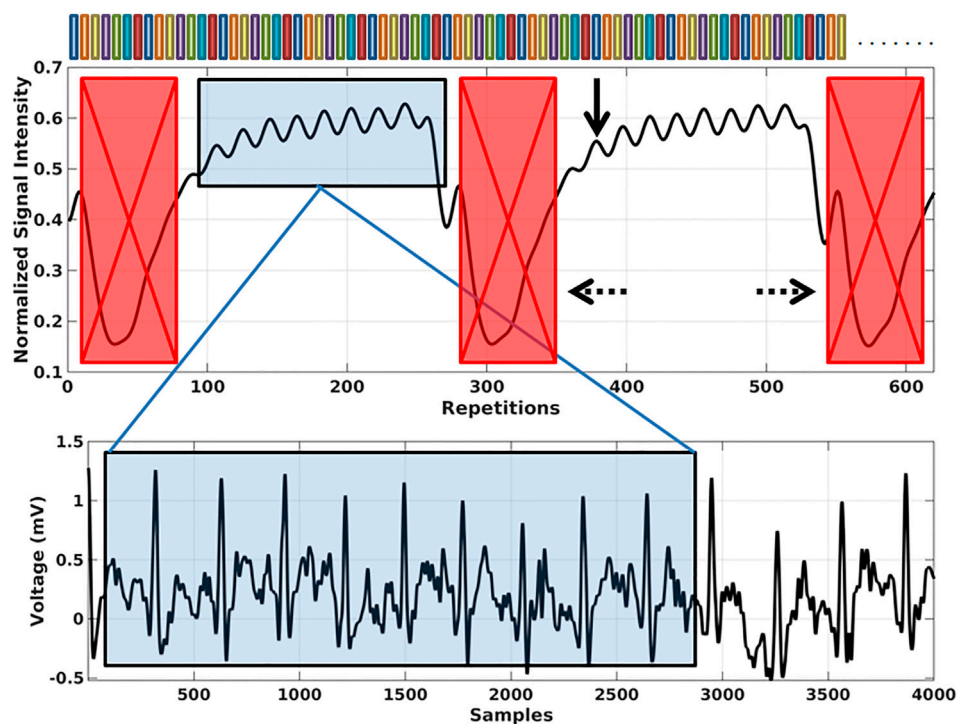


FIGURE 2

Representative image showing the cardiac and respiratory motion modulations in a filtered  $k_0$ -navigator signal. During the retrospective sorting of the main SoS-4D-flow radial spokes, the inspiration cycles and their corresponding radial spokes were discarded (dashed arrows). The peaks of the cardiac modulations were considered as the onset of the heart cycles and the radial spokes were sorted accordingly (solid arrow). The color bars on top represent different radial spokes.

Eventually, the total variation compressed sensing (CSTV) reconstruction algorithm was applied along the space, time, and velocity domains using the Berkeley Advanced Reconstruction Toolbox (BART) [20] and the corresponding velocity maps were calculated by Eqs 1–3. To adjust for the coil sensitivities, the eigenvalue-based iterative self-consistent parallel imaging reconstruction algorithm (ESPIRiT) was applied [21].

### 2.3.2.2 Cartesian-4D-flow

Since the sequence was prospectively-gated, it was not necessary to sort out the raw-data. The applied reconstruction pipeline was the same as for the SoS-4D-flow *in-vivo* experiments; i.e. all data were reconstructed using CSTV plus ESPIRiT, and the corresponding velocity maps were calculated by Eqs 1–3

## 2.4 Velocity analysis

### 2.4.1 In-vitro data

#### 2.4.1.1 Segmentation

An in-house developed semi-automatic segmentation algorithm (using the simultaneous information of the complex

images and velocity maps) was applied to label the stationary and dynamic regions within the *in-vitro* data. All labels were validated visually to ensure for the accuracy of segmentation. In the phantom data, the first and the last 20% of slices along the Z direction were discarded to mitigate the bias of RF imperfections (i.e., the middle 60% of 3D-stacks were extracted and entered statistics).

#### 2.4.1.2 Static phantom

The main purpose of using the static phantom was to evaluate and quantify the background velocity bias. After segmentation, the L2-norms of the velocity maps (i.e., velocity magnitudes) were calculated in both sequences (i.e., SoS-4D-flow and Cartesian-4D-flow), and the mean and maximum background velocity changes were compared statistically. A regression analysis between the maximum velocity and different VENC values was performed in both techniques.

#### 2.4.1.3 Flowing water phantom

The principle goal of using the flowing water phantom was to investigate the accuracy of SoS-4D-flow in comparison to the Cartesian-4D-flow technique, as well as to evaluate the

reproducibility of the findings in the static phantom. For this purpose, first, the velocity maps were segmented for the stationary and dynamic regions semi-automatically. Second, the L2-norms of the velocity maps were calculated for both the SoS-4D-flow and Cartesian-4D-flow techniques. Third, to confirm the findings of the static phantom data, the background velocity bias was reevaluated at the stationary portion of the flowing water phantom. Fourth, to compare the VNR efficiencies at different pump speeds, the individual VNRs for both sequences were calculated at the flow rates of 200, 400, 600, and 800 ml/s and were eventually summed-up. The final sum value was used for VNR comparisons. Fifth, to investigate the similarity of the SoS-4D-flow results with the Cartesian-4D-flow velocities, the velocity magnitudes of each technique were regressed to different pump speeds and the regression coefficient were compared. Sixth, to study the k-space trajectory effects on the spatial velocity profiles, the velocities across a representative tube (in which dynamic spins existed) were plotted with respect to their location and the spatial integrals were calculated and compared in both techniques. Last but not least, the effects of polar undersampling on the accuracy of SoS-4D-flow results were investigated by averaging and comparing their velocity values to the fully-sampled Cartesian-4D-flow results.

### 2.4.2 In-vivo data

For methodological comparison, the velocity maps of SoS-4D-flow and Cartesian-4D-flow were angulated perpendicular to the longitudinal axis of the ascending aorta (AA) and the through-plane velocity components were selected. Region-of-interests (ROI) were drawn manually at the distal AA and the peak systolic velocities ( $V_{max}$ ) were calculated and used for the statistical comparison. In addition, the velocity-time profiles were divided into the diastolic and systolic portions and were integrated over time for comparing the techniques. Finally, the background velocity was measured in the anterior chest wall (ACW) using ROI analysis at the same slice location.

## 3 Results

### 3.1 Static phantom

The concept of SoS-4D-flow was implemented on a small animal MRI scanner at 9.4T and the results were compared to those obtained by Cartesian-4D-flow. The qualitative evaluation of the velocity maps in both techniques showed a persistent 3D background velocity bias, with the slope of changes being less in SoS-4D-flow (Figure 3). The analysis of 4D flow data at different VENCs showed significantly lower (62.3% less) background velocity bias in SoS-4D-flow than in

Cartesian-4D-flow with the mean values of  $7.63 \pm 3.47$  cm/s vs.  $20.28 \pm 0.66$  cm/s respectively ( $p < 0.05$ ). The maximum background bias in SoS-4D-flow was on average  $19.507 \pm 4.23$  cm/s and significantly less than the maximum bias in the Cartesian-4D-flow results showing an average value of  $42.647 \pm 7.105$  cm/s ( $p < 0.05$ ). In both sequences, the maximum background velocity varied with different VENC values. Accordingly, the maximum velocity and the value of VENC showed a significant strong correlation in the Cartesian-4D-flow velocity maps ( $r = 0.992$ ,  $p < 0.05$ ), while no significant correlation was observed in the SoS-4D-flow data ( $r = 0.443$ ,  $p > 0.05$ ).

### 3.2 Flowing water phantom

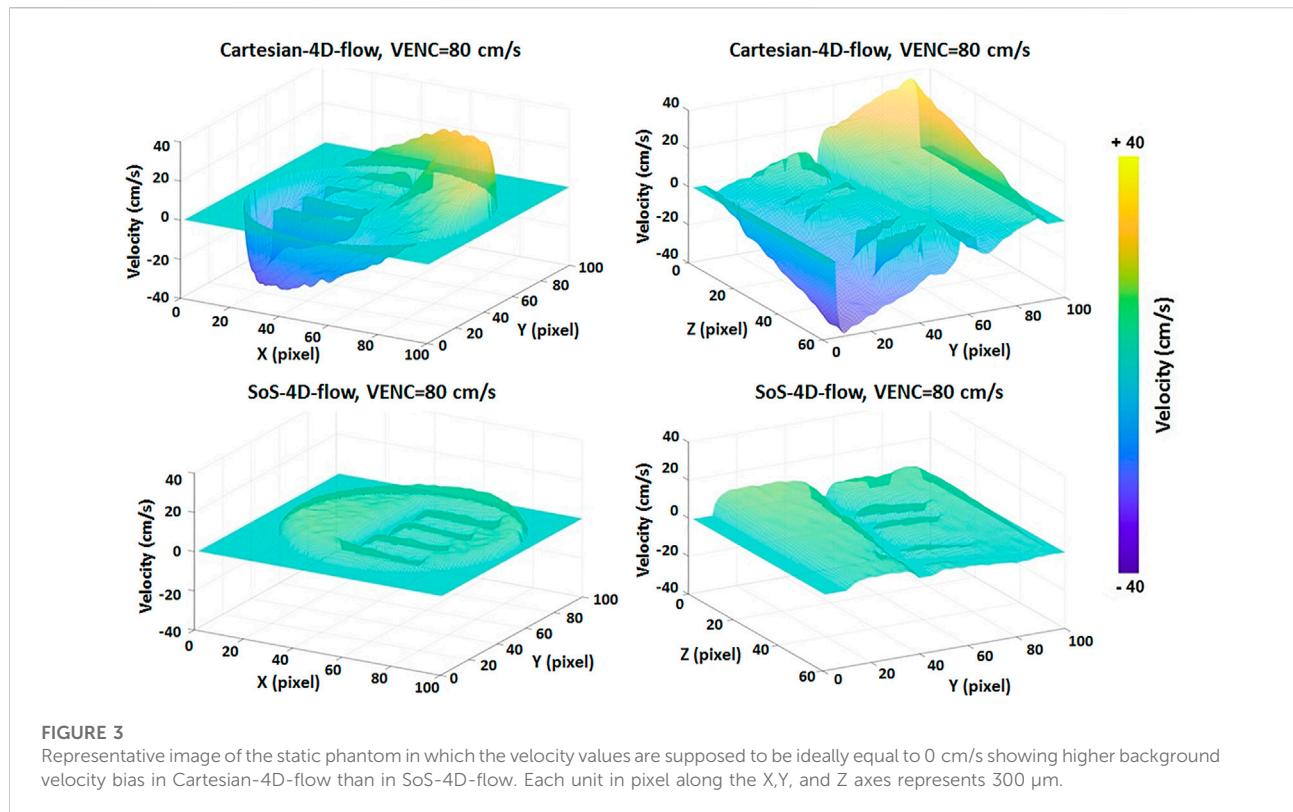
In the flow phantom, consisting of four straight tubes, our analysis showed a background velocity bias comparable to the findings in the static phantom; i.e., the averaged velocity bias in SoS-4D-flow was significantly less (56.7%) than the value inspected in Cartesian-4D-flow ( $10.75 \pm 0.05$  vs.  $24.87 \pm 0.12$  cm/s, respectively,  $p < 0.05$ ). The SoS-4D-flow acquisition with  $US = 3.15$  provided the same scan time as the fully-sampled Cartesian-4D-flow but resulted in an acceptable background velocity bias equal to  $9.90 \pm 0.11$  cm/s. The sum of VNRs (over the flow rates of 200, 400, 600 and 800 ml/s) in Cartesian-4D-flow was considerably less than the sum of VNRs in SoS-4D-flow with the values of 9.911 vs. 21.57 respectively. The sum of VNRs in the SoS-4D-flow acquisition with  $US = 3.15$  was 23.25.

In addition, a significantly strong correlation was observed between the L2-norm of velocity values in the fully-sampled SoS-4D-flow and the Cartesian-4D-flow data over the pump speeds of 200–800 ml/s ( $r = 0.994$ ,  $p < 0.05$ ). Furthermore, a strong association was observed between the velocity values measured by the undersampled SoS-4D-flow with  $US = 3.15$  and the Cartesian-4D-flow technique ( $r = 0.994$ ,  $p < 0.05$ ). Nevertheless, the agreement between the SoS-4D-flow (with and without US) and the Cartesian-4D-flow technique was reduced at slow velocities (Figure 4E).

With respect to the effect of polar undersampling on the accuracy of velocity maps, neither an underestimation nor overestimation was observed in the SoS-4D-flow velocity values at different US factors in the range of 1.0–8.0, showing an averaged velocity value of  $92.27 \pm 1.08$  cm/s in comparison to the velocity value of 93.52 cm/s measured by the fully-sampled Cartesian-4D-flow technique (Table 2).

The shape of the spatial velocity profiles in the SoS-4D-flow velocity maps (with  $US = 1$  and  $US = 3.15$ ) was preserved in comparison to the Cartesian-4D-flow technique; i.e., the spatial integral of the velocities measured by the fully-sampled SoS-4D-flow, undersampled SoS-4D-flow (with  $US = 3.15$ ), and the fully-sampled Cartesian-4D-flow technique were 931.20, 908.78 and 911.91 cm/s respectively at the pump speed of 800 ml/s, while they changed to 266.61, 262.53 and 266.23 cm/s at the pump speed of 200 ml/s respectively (Figure 4A–D).

In regard to the velocity visualization, the background velocity field imposed a systematic vector alteration in the



Cartesian-4D-flow results, influencing both the magnitudes and the directions of the corresponding velocity vector fields, which was more prominent at slow pump speeds (Figure 5).

### 3.3 In-Vivo analysis

For *in-vivo* blood flow analysis, the SoS-4D-flow sequence was extended by  $k_0$ -navigation and CSTV reconstruction. No significant differences were observed between the  $V_{\max}$  values of the SoS-4D-flow and Cartesian-4D-flow results in AA ( $91.83 \pm 13.18$  vs.  $92.61 \pm 9.57$  cm/s respectively,  $p > 0.05$ ). However, the sum of the diastolic velocities differed significantly between both sequences (SoS-4D-flow:  $24.23 \pm 5.41$  vs. Cartesian-4D-flow:  $82.88 \pm 30.38$  cm/s,  $p < 0.05$ ). Nevertheless, the sum of the systolic velocities showed no significant difference between the SoS-4D-flow and Cartesian-4D-flow result ( $449.96 \pm 88.13$  vs.  $520.83 \pm 73.29$  cm/s respectively,  $p > 0.05$ ) (Figure 6, E). The velocity-time curves of both the techniques showed a significant linear correlation ( $r = 0.995$ ,  $p < 0.05$ ) to each other. The averaged background velocity over ACW was significantly less in the SoS-4D-flow velocity maps compared to the Cartesian-4D-flow data with the average values of  $3.29 \pm 0.95$  vs.  $14.29 \pm 5.49$  cm/s respectively ( $p < 0.05$ ). Qualitatively, the streamline directions of Cartesian-4D-flow were influenced by the concomitant field *in-vivo* showing distracted flow directions in aorta, while the streamlines of the SoS-4D-flow techniques were preserved and represented the

expected orientations (Figure 6A–D). The average scan time of the Cartesian-4D-flow and the SoS-4D-flow technique were  $70.32 \pm 4.33$  and  $68.74 \pm 8.73$  minutes orderly.

## 4 Discussion

Historically, the concept of 4D-flow imaging emerged in the late 1990s [22, 23] and has been continuously refined through improvements in velocity encoding methods [4, 24–27], spatial encoding trajectories [7, 28–31] and reconstruction pipelines [32, 33]. It has already been reported that TE shortening could reduce intravoxel-dephasing of higher-order motions, such as found in turbulent flows [34, 35]. Accordingly, O'Brien et al. introduced a UTE-2D-flow sequence with  $TE \approx 0.65$  ms to recover the signal from high-velocity turbulent jets after the presence of stenosis [36].

With the initial introduction of the stack-of-stars phase contrast angiography at 3.0T by Kecskemeti et al., the minimum achievable TE was 3.7 ms due to full spoke readout from  $-k$  to  $+k$  [37], which was considered an appropriate TE for angiographic purposes but not for velocity mapping. Kadbi et al. adopted the concept of center-out acquisition from [36] and combined it with [37] to design a SoS-4D-flow with  $TE \approx 1$  ms at 1.5T [6]. However, their study was mainly investigated *in-vitro* and did not include any comprehensive evaluations *in-vivo*. Up

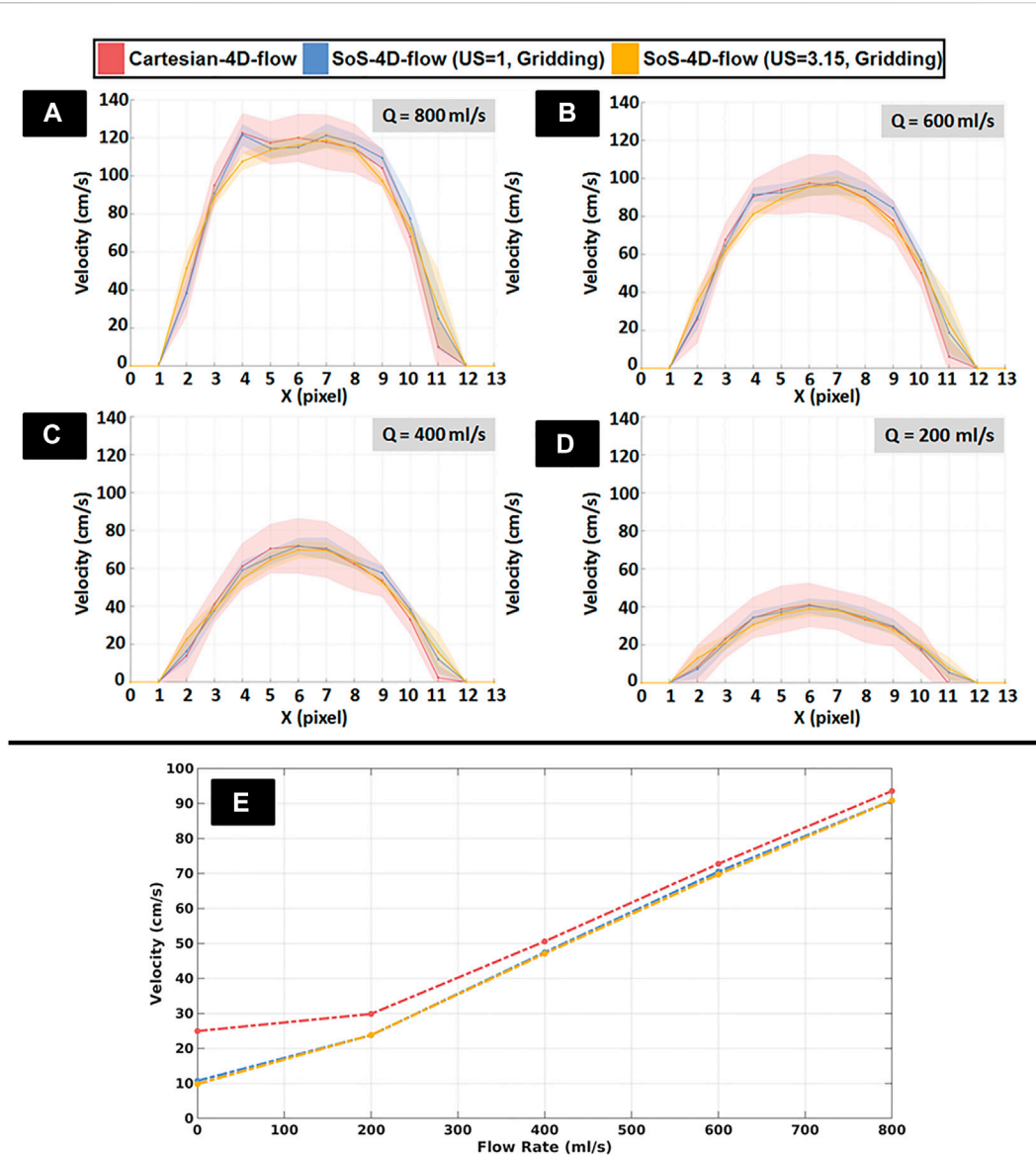


**FIGURE 4** (A–D) Representative spatial velocity profiles perpendicular to the long axis of a representative tube (solid lines: mean velocity, shades: standard deviation) obtained from fully sampled SoS-4D-flow, undersampled SoS-4D-flow with an undersampling (US) factor of  $\pi$ , and Cartesian-4D-flow data at different pump speeds (Q) ranging from 200 to 800 ml/s. Each unit in pixel along the X axis represents  $300\mu\text{m}$ . (E) Representative plot showing the velocity values obtained by the fully-sampled SoS-4D-flow, undersampled SoS-4D-flow, and the fully-sampled Cartesian-4D-flow technique at different flow rates (i.e., pump speeds).

to our knowledge, the application of the center-out SoS-4D-flow sequence has not been investigated in UHFs, neither in human nor small animal imaging.

Since the prospectively-triggered Cartesian-4D-flow velocity mapping requires long gradient duration as well as a bipolar readout gradient to cover  $-k$  to  $+k$  line by line, its typical TEs are long enough to be considered as an disadvantage in the regions of higher blood flow at 9.4T because of signal cancellation. For this purpose, we implemented a golden-angle center-out SoS-4D-

flow sequence at 9.4T with reduced TE  $\approx 1$  ms and evaluated it *in-vitro* and *in-vivo*.

Our *in-vitro* investigations in the static phantom showed a notable background velocity deviation in the Cartesian-4D-flow velocity maps, which was dependent on the location of the voxel and was persistent in different VENC values, tending to increase with higher velocity sensitizing gradient amplitudes. Since the reduction of TE in UHF systems is crucial to compensate for the intensified intravoxel-dephasing, it is a common practice to overlap all gradient



TABLE 2 *In-vitro* comparison of the velocity values of multiple SoS-4D-flow measurements with different undersampling factors to the reference value obtained by the fully-sampled Cartesian-4D-flow technique.

Sequence	Scan time (minute: Second)	US	Velocity (cm/s)
Cartesian-4D-flow	4:00	1.0	93.52 ± 36.90
SoS-4D-flow	12:33	1.0	90.81 ± 33.18
SoS-4D-flow	8:24	1.5	92.09 ± 30.63
SoS-4D-flow	6:19	2.0	91.54 ± 29.29
SoS-4D-flow	5:02	2.5	92.28 ± 28.11
SoS-4D-flow	4:09	3.0	91.39 ± 26.21
SoS-4D-flow	3:36	3.5	92.27 ± 25.08
SoS-4D-flow	3:07	4.0	93.53 ± 23.92
SoS-4D-flow	2:48	4.5	92.69 ± 23.17
SoS-4D-flow	2:28	5.0	93.85 ± 22.91
SoS-4D-flow	2:19	5.5	94.88 ± 23.11
SoS-4D-flow	2:04	6.0	92.28 ± 21.18
SoS-4D-flow	1:55	6.5	91.24 ± 20.60
SoS-4D-flow	1:45	7.0	92.11 ± 21.21
SoS-4D-flow	1:40	7.5	90.81 ± 21.26
SoS-4D-flow	1:36	8.0	92.26 ± 21.63

(US, undersampling factor).

events (i.e., slice, phase, readout, etc.) in the design of Cartesian sequences. The design of the standard Cartesian-4D-flow sequence at 9.4 T is not an exception from this convention. Since all gradient events overlap along the X, Y, and Z directions in the Cartesian-4D-flow technique, the net gradient amplitude along each physical coordinate is very strong. This led to the formation of a strong concomitant field (Maxwell field) and consequently to a huge phase drift throughout the object—which is the main source of the observed significant background velocity bias in the Cartesian-4D-flow data. As reported by Bernstein et al. [38] and Norris et al. [39], the gradient polarity does not have any influence on the phase drift and thus the reconstruction of the velocity maps using Eqs 1–3 could not unwrap and correct the signal. Based on [38], the velocity drift has to be dependent on both the voxel location and the net gradient amplitude along the physical axes, which was in accordance with our observations; i.e. we observed that the strongest velocity drift existed at the diagonal axis from the gradient isocenter at the end points of FOVs. The background velocity bias due to the Maxwell field was significantly ( $p < 0.05$ ) reduced in SoS-4D-flow since it had fewer overlapping gradients.

Similar to the static phantom, a big velocity drift was observed in the results of the flowing water phantom. When a comparison was drawn between the velocity maps acquired by SoS-4D-flow and Cartesian-4D-flow at different pump speeds, we observed that the Maxwell field changed the streamline directions in Cartesian-4D-flow at slow flow rates (i.e., slow velocities). However no obvious changes were detected in the streamlines reconstructed from the SoS-4D-flow data at the same pump speed (Figure 5). Therefore, it is predictable that the presence of strong concomitant fields in the Cartesian-4D-

flow sequence at short TE can limit its application at UHFs for imaging at high resolutions and low VENC values since both conditions increase the net gradient amplitudes. Additionally, we observed that the effect of the concomitant field on the total velocity vector field of the Cartesian-4D-flow technique was still persistent but less prominent at fast flow rates (i.e., at fast velocities) (Figure 5).

Our *in-vivo* findings were in accordance with the *in-vitro* results, with respect to a higher background velocity observed in Cartesian-4D-flow compared to SoS-4D-flow. By having a closer look at the corresponding velocity-time curves (Figure 6E), the difference in the hemodynamic profiles was more prominent during the diastolic period than in the systole, suggesting that for the evaluation of slow velocities (such as the diastolic velocity profiles) the application of SoS-4D-flow can be superior to Cartesian-4D-flow at UHFs. Since the reconstruction algorithm of both techniques was the same, the difference could not originate from the reconstruction pipeline but rather from the sequence itself. Furthermore, the integration of the SoS-4D-flow technique with the  $k_0$ -navigator pulse and retrospective reconstruction could increase the quality of its velocity maps in two additional ways; (A) the poor quality ECG was replaced by a strong navigator signal, which decreased the possible errors originating from the triggering method; (B) for retrospective reconstructions, we scanned the whole k-space with 25 repetition, then sorted the signals and averaged each sorted k-space over all the 25 repetitions. This part of the pipeline could reduce the thermal noise in the source complex images and could increase the VNR in the final velocity maps.

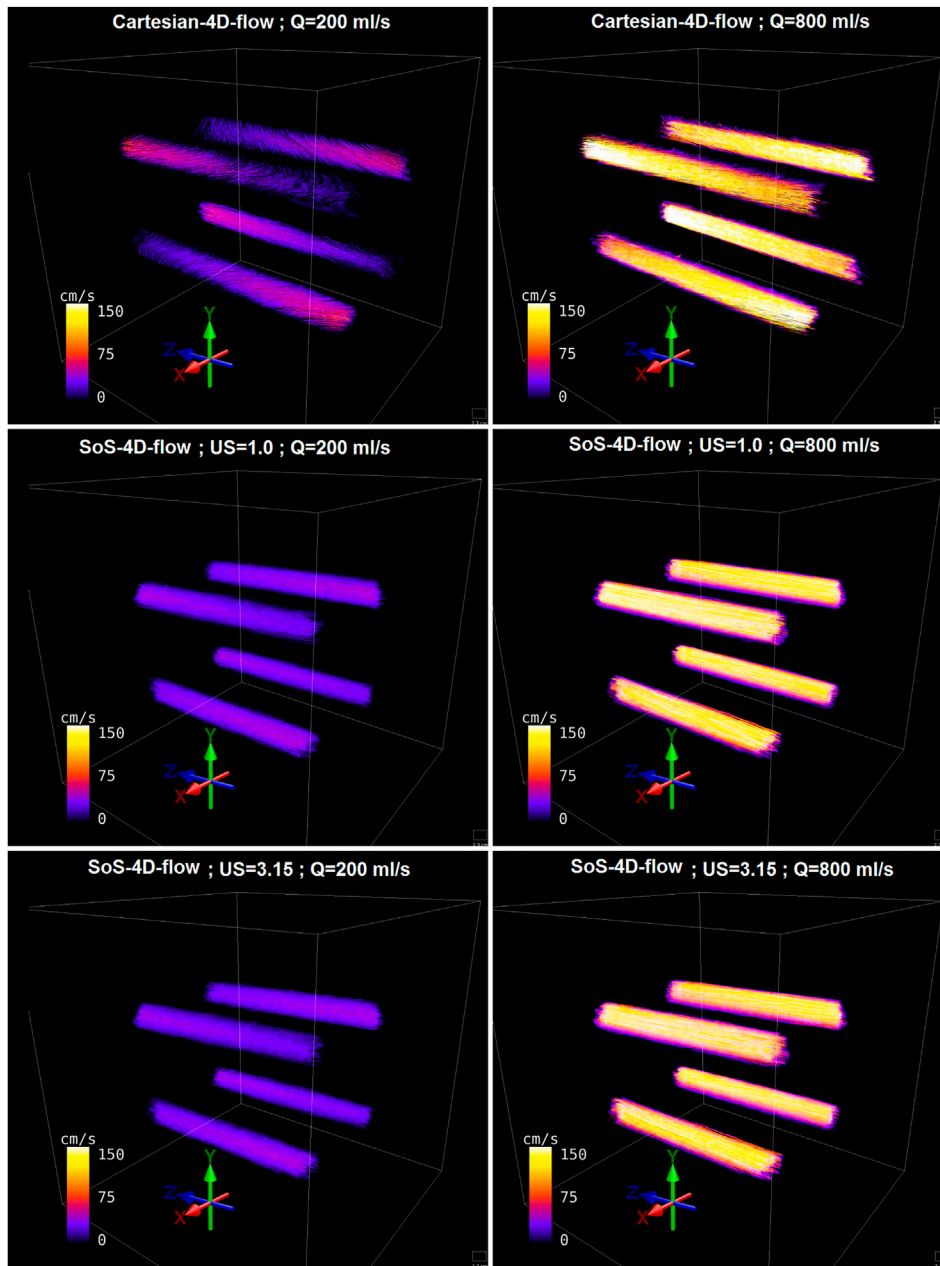


**FIGURE 5**  
 Representative streamline visualization of the *in-vitro* flowing water phantom reconstructed from fully-sampled SoS-4D-flow, undersampled SoS-4D-flow (by a factor of  $\pi$ ), and Cartesian-4D-flow data at high and low pump speeds (Q value).

According to [40, 41], anesthesia of small animals using Isoflurane can influence the cardiac physiology and the corresponding hemodynamics; hence, shorter scan times are always preferable for cardiac magnetic resonance. In this regard and in comparison to the other sophisticated sequences such as UTE-4D-flow (which covers the whole k-space center-out radially), we believe that the application of SoS-4D-flow could be more advantageous despite of its less expected VNR. Since the size of

the imaging matrix is a determinant factor on the number of the required projections in UTE-4D-flow; high resolution imaging with large field-of-views (FOV) could limit the application of UTE-4D-flow due to time constraints. For instance, in a previous investigation on the UTE-4D-flow technique, the total scan time at the resolution of the current study (i.e.,  $230 \mu\text{m}$ ) was  $\approx 2 \text{ h}$  with  $TR = 3.1 \text{ ms}$  [3], while the total scan time of SoS-4D-flow was  $\approx 68 \text{ minutes}$  with  $TR = 6 \text{ ms}$  (i.e., the hybrid characteristics of SoS-4D-flow could save time

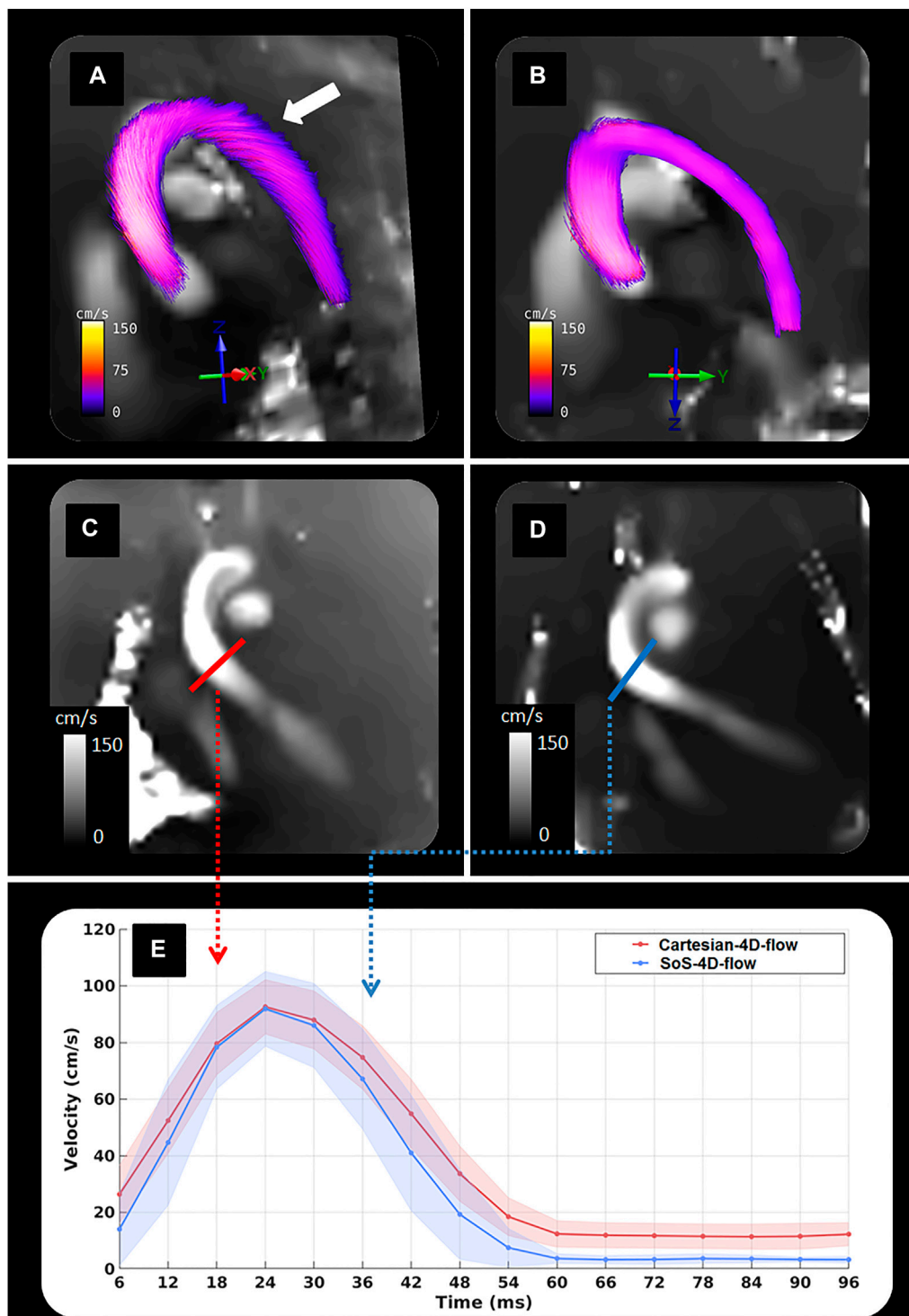


**FIGURE 6**

Representative figure showing (A) Streamline visualization of an *in-vivo* data obtained by Cartesian-4D-flow; (B) Streamline visualization of an *in-vivo* data obtained by SoS-4D-flow; (C) A velocity map of an *in-vivo* data acquired by Cartesian-4D-flow; (D) A velocity map of an *in-vivo* data measured by SoS-4D-flow; (E) Velocity-time curves at the cross-section of the distal ascending aorta obtained by the  $k_0$ -navigated SoS-4D-flow and the prospectively-triggered Cartesian-4D-flow technique. Please note that the strong background velocity in the Cartesian-4D-flow data has influenced the streamline orientation in aorta (solid white arrow), while the streamline quality is well-preserved in the SoS-4D-flow results.

since the  $\pi$  factor of additional projections along the slice/slab directions is not further required). It is not yet known whether the simultaneous applications of three readout gradients in the UTE-4D-flow technique have any significant impact on the formation of Maxwell fields or not, especially at high resolutions. Thus, further investigations are recommended to compare the Maxwell fields in the SoS-4D-flow sequence with those in the UTE-4D-flow technique. For an accurate comparison, according to the methodology presented in [3], we suggest to use a spatially nonselective RF pulse in the absence of any slice/slab selection gradients to minimize TE and the net gradient amplitude in SoS-4D-flow. Since UTE-4D-flow is based on the Kooshball trajectory, it would be invaluable to additionally investigate the effects of the polar undersampling on the accuracy of the resultant velocity maps in comparison to the fully accelerated SoS-4D-flow technique. However, this investigation was not in the scope of this research and will require further studies.

Since we used no Cartesian acceleration along the  $k_z$ -direction in SoS-4D-flow (i.e., we used only polar undersampling in the  $k_{xy}$  plane), we decided to apply no Cartesian undersampling in the reference 4D-flow measurements (i.e., Cartesian-4D-flow). This approach could eliminate the corresponding confounding factors in the final statistical analysis. Accordingly, it is not clear how the results of those two methods would deviate if a full Cartesian acceleration was applied. Hence, we suggest a deeper investigation to address this issue.

Physically, there are only two remedies to reduce the concomitant fields in Cartesian-4D-flow (A) to separate the imaging and velocity encoding gradients from each other, which increases TE and signal loss at UHFs, especially in the regions with the higher order blood flow; (B) to use coarser spatial resolutions or higher VENC values to use a weaker gradient strength. Despite of the applicability of those approaches in big *in-vivo* objects (such as humans), they limit the application of the Cartesian-4D-flow in small animal imaging since high resolutions and short TE are always required. Analytically, the effect of concomitant fields can also be corrected by solving a fitting problem; nevertheless, the sole application of the model-based correction methods is subject to inaccuracies [42]. Accordingly, the model-based corrections can add bias into the regions where real velocities exist. Thus, the optimum correction of the Maxwell field additionally necessitates modifying the gradient events [38]. Based on this, SoS-4D-flow has little gradient overlaps and results in a negligible concomitant field. In addition, it benefits from a short TE at UHFs, which preserves the accuracy of estimated velocities [6]. To this end, we come into the conclusion that the SoS-4D-flow technique is not only suitable to accurately quantify fast velocities requiring short TEs, but also is a precise method for the estimation of a wide range of velocities including slow flows.

## Data availability statement

The raw data supporting the conclusion of this article will be made available by the authors, without undue reservation.

## Ethics statement

The animal study was reviewed and approved by the State Office for Food Safety and Consumer Protection (TLLV, Bad Langensalza, Germany).

## Author contributions

AN: Conceptualization, sequence design, data acquisition, image reconstruction, image and statistical analysis, validation, visualization, original draft preparation, review and editing. MK: Conceptualization, sequence design, image reconstruction, image analysis, validation, review and editing. ME: data acquisition, validation, review and editing. K-HH: sequence design, validation, review and editing. SL: Image analysis, review and editing. LL: Image analysis, review and editing. SM: Image and statistical analysis, validation, review and editing. JR: Conceptualization, validation, review and editing, project administration. VH: Conceptualization, sequence design, data acquisition, image and statistical analysis, validation, review and editing, project administration. All authors have read and agreed to the published version of the manuscript.

## Funding

This study was supported by the German Research Foundation (Deutsche Forschungsgemeinschaft/DFG, Project-ID: 468824876 granted to VH and LL).

## Acknowledgments

Parts of this work will be used in the doctoral thesis of AN. We would like to thank Van Nhat Minh Vo for his support.

## Conflict of interest

The authors declare that the research was conducted in the absence of any commercial or financial relationships that could be construed as a potential conflict of interest.

## Publisher's note

All claims expressed in this article are solely those of the authors and do not necessarily represent those of their affiliated organizations, or those of the publisher, the editors and the reviewers. Any product that may be evaluated in this article, or claim that may be made by its manufacturer, is not guaranteed or endorsed by the publisher.

## References

- Dyverfeldt P, Bissell M, Barker AJ, Bolger AF, Carlhäll C-J, Ebbers T, et al. 4D flow cardiovascular magnetic resonance consensus statement. *J Cardiovasc Magn Reson* (2015) 17(1):72. doi:10.1186/s12968-015-0174-5
- Nayak KS, Nielsen J-F, Bernstein MA, Markl M, Gatehouse P D, Botnar R M, et al. Cardiovascular magnetic resonance phase contrast imaging. *J Cardiovasc Magn Reson* (2015) 17(1):71. doi:10.1186/s12968-015-0172-7
- Krämer M, Motaal AG, Herrmann KH, Löffler B, Reichenbach JR, Strijkers GJ, et al. Cardiac 4D phase-contrast CMR at 9.4 T using self-gated ultra-short echo time (UTE) imaging. *J Cardiovasc Magn Reson* (2017) 19(1):39. doi:10.1186/s12968-017-0351-9
- Pelc NJ, Bernstein MA, Shimakawa A, Glover GH. Encoding strategies for three-direction phase-contrast MR imaging of flow. *J Magn Reson Imaging* (1991) 1(4):405–13. doi:10.1002/jmri.1880010404
- Dyverfeldt P, Hope MD, Tseng EE, Saloner D. Magnetic resonance measurement of turbulent kinetic energy for the estimation of irreversible pressure loss in aortic stenosis. *JACC: Cardiovasc Imaging* (2013) 6(1):64–71. doi:10.1016/j.jcmg.2012.07.017
- Kadbi M, Negahdar MJ, Cha J, Traugher M, Martin P, Stoddard MF, et al. 4D UTE flow: A phase-contrast MRI technique for assessment and visualization of stenotic flows. *Magn Reson Med* (2015) 73(3):939–50. doi:10.1002/mrm.25188
- Braig M, Menza M, Leupold J, LeVan P, Feng L, Ko C-W, et al. Analysis of accelerated 4D flow MRI in the murine aorta by radial acquisition and compressed sensing reconstruction. *NMR Biomed* (2020) 33(11):e4394. doi:10.1002/nbm.4394
- Bock J, Töger J, Bidhult S, Markenroth Bloch K, Arvidsson P, Kanski M, et al. Validation and reproducibility of cardiovascular 4D-flow MRI from two vendors using 2 × 2 parallel imaging acceleration in pulsatile flow phantom and *in vivo* with and without respiratory gating. *Acta Radiol* (2018) 60(3):327–37. doi:10.1177/0284185118784981
- Braig M, Leupold J, Menza M, Russe M, Ko C-W, Hennig J, et al. Preclinical 4D-flow magnetic resonance phase contrast imaging of the murine aortic arch. *PLOS ONE* (2017) 12(11):e0187596. doi:10.1371/journal.pone.0187596
- Bovenkamp PR, Brix T, Lindemann F, Holtmeier R, Abdurrachim D, Kuhlmann MT, et al. Velocity mapping of the aortic flow at 9.4 T in healthy mice and mice with induced heart failure using time-resolved three-dimensional phase-contrast MRI (4D PC MRI). *Magn Reson Mater Phys* (2015) 28(4):315–27. doi:10.1007/s10334-014-0466-z
- Giese D, Wong J, Greil GF, Buehrer M, Schaeffter T, Kozerke S. Towards highly accelerated Cartesian time-resolved 3D flow cardiovascular magnetic resonance in the clinical setting. *J Cardiovasc Magn Reson* (2014) 16(1):42. doi:10.1186/1532-429x-16-42
- Walheim J, Gotschy A, Kozerke S. On the limitations of partial Fourier acquisition in phase-contrast MRI of turbulent kinetic energy. *Magn Reson Med* (2019) 81(1):514–23. doi:10.1002/mrm.27397
- Bruschewski M, Kolkmann H, John K, Grundmann S. Phase-contrast single-point imaging with synchronized encoding: A more reliable technique for *in vitro* flow quantification. *Magn Reson Med* (2019) 81(5):2937–46. doi:10.1002/mrm.27604
- Pipe JG, Menon P. Sampling density compensation in MRI: Rationale and an iterative numerical solution. *Magn Reson Med* (1999) 41(1):179–86. doi:10.1002/(sici)1522-2594(199901)41:1<179:aid-mrm25>3.0.co;2-v
- Zwart NR, Johnson KO, Pipe JG. Efficient sample density estimation by combining gridding and an optimized kernel. *Magn Reson Med* (2012) 67(3):701–10. doi:10.1002/mrm.23041
- Herrmann KH, Krämer M, Reichenbach JR. Time efficient 3D radial UTE sampling with fully automatic delay compensation on a clinical 3T MR scanner. *PLoS One* (2016) 11(3):e0150371. doi:10.1371/journal.pone.0150371
- Krämer M, Herrmann K-H, Biermann J, Freiburger S, Schwarzer M, Reichenbach JR. Self-gated cardiac Cine MRI of the rat on a clinical 3 T MRI system. *NMR Biomed* (2015) 28(2):162–7. doi:10.1002/nbm.3234
- Larson AC, White RD, Laub G, McVeigh ER, Li D, Simonetti OP. Self-gated cardiac cine MRI. *Magn Reson Med* (2004) 51(1):93–102. doi:10.1002/mrm.10664
- Duyn JH, Yang Y, Frank JA, van der Veen JW. Simple correction method for k-space trajectory deviations in MRI. *J Magn Reson* (1998) 132(1):150–3. doi:10.1006/jmre.1998.1396
- M Uecker, F Ong, JI Tamir, D Bahri, P Virtue, JY Cheng, et al. editors. “Berkeley advanced reconstruction Toolbox,” in International Society of Magnetic Resonance in Medicine 2015, 23 (2015). p. 2486.
- Uecker M, Lai P, Murphy MJ, Virtue P, Elad M, Pauly JM, et al. ESPIRiT—an eigenvalue approach to autocalibrating parallel MRI: Where SENSE meets GRAPPA. *Magn Reson Med* (2014) 71(3):990–1001. doi:10.1002/mrm.24751
- Wigström L, Ebbers T, Fyrenius A, Karlsson M, Engvall J, Wranne B, et al. Particle trace visualization of intracardiac flow using time-resolved 3D phase contrast MRI. *Magn Reson Med* (1999) 41(4):793–9. doi:10.1002/(sici)1522-2594(199904)41:4<793:aid-mrm19>3.0.co;2-2
- Bogren HG, Buonocore MH. 4D magnetic resonance velocity mapping of blood flow patterns in the aorta in young vs. elderly normal subjects. *J Magn Reson Imaging* (1999) 10(5):861–9. doi:10.1002/(sici)1522-2586(199911)10:5<861:aid-jmri35>3.0.co;2-e
- Conturo TE, Robinson BH. Analysis of encoding efficiency in MR imaging of velocity magnitude and direction. *Magn Reson Med* (1992) 25(2):233–47. doi:10.1002/mrm.1910250203
- Lee AT, Pike GB, Pelc NJ. Three-point phase-contrast velocity measurements with increased velocity-to-noise ratio. *Magn Reson Med* (1995) 33(1):122–6. doi:10.1002/mrm.1910330119
- Herment A, Mousseaux E, Jolivet O, DeCesare A, Frouin F, Todd-Pokropek A, et al. Improved estimation of velocity and flow rate using regularized three-point phase-contrast velocimetry. *Magn Reson Med* (2000) 44(1):122–8. doi:10.1002/1522-2594(200007)44:1<122:aid-mrm18>3.0.co;2-c
- Nett EJ, Johnson KM, Frydrychowicz A, Del Rio AM, Schrauben E, Francois CJ, et al. Four-dimensional phase contrast MRI with accelerated dual velocity encoding. *J Magn Reson Imaging* (2012) 35(6):1462–71. doi:10.1002/jmri.23588
- Negahdar MJ, Kadbi M, Kendrick M, Stoddard MF, Amini AA. 4D spiral imaging of flows in stenotic phantoms and subjects with aortic stenosis. *Magn Reson Med* (2016) 75(3):1018–29. doi:10.1002/mrm.25636
- Corrado PA, Medero R, Johnson KM, François CJ, Roldán-Alzate A, Wieben O. A phantom study comparing radial trajectories for accelerated cardiac 4D flow MRI against a particle imaging velocimetry reference. *Magn Reson Med* (2021) 86(1):363–71. doi:10.1002/mrm.28698
- Peper ES, Gottwald LM, Zhang Q, Coolen BF, van Ooij P, Nederveen AJ, et al. Highly accelerated 4D flow cardiovascular magnetic resonance using a pseudo-spiral Cartesian acquisition and compressed sensing reconstruction for carotid flow and wall shear stress. *J Cardiovasc Magn Reson* (2020) 22(1):7. doi:10.1186/s12968-019-0582-z
- Kolbitsch C, Bastkowski R, Schäffter T, Prieto Vasquez C, Weiss K, Maintz D, et al. Respiratory motion corrected 4D flow using golden radial phase encoding. *Magn Reson Med* (2020) 83(2):635–44. doi:10.1002/mrm.27918
- Ma LE, Markl M, Chow K, Huh H, Forman C, Vali A, et al. Aortic 4D flow MRI in 2 minutes using compressed sensing, respiratory controlled adaptive k-space reordering, and inline reconstruction. *Magn Reson Med* (2019) 81(6):3675–90. doi:10.1002/mrm.27684
- Pathrose A, Ma L, Berhane H, Scott MB, Chow K, Forman C, et al. Highly accelerated aortic 4D flow MRI using compressed sensing: Performance at different acceleration factors in patients with aortic disease. *Magn Reson Med* (2021) 85(4):2174–87. doi:10.1002/mrm.28561
- O’Brien KR, Cowan BR, Jain M, Stewart RA, Kerr AJ, Young AA. MRI phase contrast velocity and flow errors in turbulent stenotic jets. *J Magn Reson Imaging* (2008) 28(1):210–8. doi:10.1002/jmri.21395
- Ståhlberg F, Thomsen C, Söndergaard L, Henriksen O. Pulse sequence design for MR velocity mapping of complex flow: Notes on the necessity of low echo times. *Magn Reson Imaging* (1994) 12(8):1255–62. doi:10.1016/0730-725x(94)90090-e
- O’Brien KR, Myerson SG, Cowan BR, Young AA, Robson MD. Phase contrast ultrashort TE: A more reliable technique for measurement of high-velocity turbulent stenotic jets. *Magn Reson Med* (2009) 62(3):626–36. doi:10.1002/mrm.22051
- Kecskemeti S, Johnson K, Wu Y, Mistretta C, Turski P, Wieben O. High resolution three-dimensional cine phase contrast MRI of small intracranial aneurysms using a stack of stars k-space trajectory. *J Magn Reson Imaging* (2012) 35(3):518–27. doi:10.1002/jmri.23501
- Bernstein MA, Zhou XJ, Polzin JA, King KF, Ganin A, Pelc NJ, et al. Concomitant gradient terms in phase contrast MR: Analysis and correction. *Magn Reson Med* (1998) 39(2):300–8. doi:10.1002/mrm.1910390218
- Norris DG, Hutchison JMS. Concomitant magnetic field gradients and their effects on imaging at low magnetic field strengths. *Magn Reson Imaging* (1990) 8(1):33–7. doi:10.1016/0730-725x(90)90209-k
- Roth DM, Swaney JS, Dalton ND, Gilpin EA, Ross J, Jr. Impact of anesthesia on cardiac function during echocardiography in mice. *Am J Physiology-Heart Circulatory Physiol* (2002) 282(6):H2134–40. doi:10.1152/ajpheart.00845.2001
- Berry CJ, Thedens DR, Light-McGroary K, Miller JD, Kutschke W, Zimmerman KA, et al. Effects of deep sedation or general anesthesia on cardiac function in mice undergoing cardiovascular magnetic resonance. *J Cardiovasc Magn Reson* (2009) 11(1):16. doi:10.1186/1532-429x-11-16
- Sträter A, Huber A, Rudolph J, Berndt M, Rasper M, Rummeny EJ, et al. 4D-Flow MRI: Technique and applications. *Rofo* (2018) 190(11):1025–35. doi:10.1055/a-0647-2021